*forests*

MDPI

*Article*

# Using a Phenocamera to Monitor Urban Forest Phenology

**Kaidi Zhang [1,2,3,*], Jinmiao Bai [1,4] and Jun Gao [1,4,*]**

[1] School of Environmental and Geographical Sciences, Shanghai Normal University, 100 Guilin Road, Xuhui District, Shanghai 200234, China; mmmlock@outlook.com
[2] Anhui Province Key Laboratory of Atmospheric Science and Satellite Remote Sensing, Anhui Institute of Meteorological Sciences, Hefei 230031, China
[3] Shouxian National Climatology Observatory, Huaihe River Basin Typical Farm Eco-Meteorological Experiment Field of CMA, Shouxian 232200, China
[4] Yangtze River Delta Urban Wetland Ecosystem National Field Scientific Observation and Research Station, Shanghai 200234, China
* Correspondence: zhangkaidi_1022@163.com or zhangkaidi@ahmi.org.cn (K.Z.); gaojun@shnu.edu.cn (J.G.)

**Abstract:** Under global climate change, fragmented urban vegetation is more susceptible to the external environment, and changes in vegetation phenology are one of the most apparent responses. In this study, phenological camera (phenocamera) photo data, Klosterman curve fitting, and a Gu model were employed to explore the phenological characteristics of an urban forest at different levels within different species. Differences between species and groups regarding the upturn date (UD), the stabilization date (SD), the downturn date (DD), the recession date (RD), and the length of the growing season (LOS) are displayed in detail. We found that the UD of *Cinnamomum camphora* groups began in late April (day of year 108th), the SD appeared in early May (121st), and the DD started in early October (283rd) and ended in late October (293rd), with an average LOS of 185 days. The phenological characteristics of the *Cinnamomum camphora* and *Bischofia polycarpa* groups differed significantly. The average LOS of *Bischofia polycarpa* was 47 days longer than that of *Cinnamomum camphora*. Between *Cinnamomum camphora* individuals and group levels, differences in the UD and the SD were not obvious, while differences in the DD, the RD, and the LOS were large (LOS > RD > DD). The LOS of *Cinnamomum camphora* was longer on the individual scale (209 days), while the average LOS on the group scale was 185 days. In conclusion, our results reflect the more refined quantitative results of urban vegetation phenology and will help to elucidate urban vegetation phenological changes, which has important theoretical and practical significance for future urban forest management practices.

**Keywords:** *Cinnamomum camphora* and *Bischofia polycarpa*; vegetation phenology; vegetation index; key phenological metrics

check for updates

Academic Editor: Jinda Qi

Received: 23 December 2024
Revised: 22 January 2025
Accepted: 23 January 2025
Published: 26 January 2025

**Citation:** Zhang, K.; Bai, J.; Gao, J. Using a Phenocamera to Monitor Urban Forest Phenology. *Forests* **2025**, *16*, 239. https://doi.org/10.3390/f16020239

**Copyright:** © 2025 by the authors. Licensee MDPI, Basel, Switzerland. This article is an open access article distributed under the terms and conditions of the Creative Commons Attribution (CC BY) license (https://creativecommons.org/licenses/by/4.0/).

## 1. Introduction

Urban areas cover less than 3% of the terrestrial Earth's surface [1,2] but accommodate 68% of the world's population, with a persistently increasing trend [3]. High-density population and intensive human activities are the main reasons for the change in urban environments, and they also form the unique microclimate environment of the city, such as the urban heat island effect (UHI) [4]. Vegetation phenology is the study of recurring patterns of plant growth and development, including, for example, the time of budburst, plant flowering, leaf greenup, and senescence [5]. It has been widely accepted that vegetation phenology is a key indicator of global climate change, which is strongly connected with warming temperatures [6–8]. Changes in the urban environment due to atmospheric,

soil, and light pollution will affect plant phenology (e.g., leaf senescence) [9], resulting in different phenology characteristics in urban ecosystems. However, our knowledge about the vegetation phenology response to urbanization under different urban morphology scenarios is still unclear, partly because of the difficulties in observing and mapping the dynamics of vegetation phenology at appropriate spatial and temporal resolutions in and around urban areas [10]. Therefore, monitoring urban vegetation phenology is important in understanding how climate change mechanisms influence vegetation cover and how plants respond to urban environmental changes.

Vegetation phenology can be observed using a variety of approaches, including the long-standing methods of field observation and remote sensing data [11,12]. Field observations, while reliable at the individual scale, are limited by range, scale, and observer variability [11,13–15]. As a result, near-surface optical imaging has become a prominent method for capturing phenological data [16,17]. Satellite-based remote sensing, offering data on a larger spatial scale through indices like NDVI and EVI, is widely used in land surface phenology (LSP) studies [12,18]. However, satellite data suffer from coarse temporal resolution and cloud contamination, which complicates the tracking of rapid phenological changes [19,20]. The application of Unmanned Aerial Vehicle (UAV) technology in urban forest monitoring is also constantly innovative because of the development of UAVs and drone technology. It efficiently collects structural and ecological data of urban forests, which not only improves the efficiency and accuracy of data collection and analysis but also expands the dimensions and application scenarios of monitoring [21–23].

In recent years, as a relatively new method of data acquisition, Phenocams have become an irreplaceable data source in the field of vegetation phenology research due to their unique small-scale and long-term monitoring capabilities, as well as the high reliability of the resulting data [24,25]. The vegetation indices from digital photographs by Phenocams can efficiently track the seasonal variations in phenology of forest ecosystem [26,27]. The GCC was correlated with canopy photosynthesis and widely applied to extract phenological events [12,27,28]. Current evidence indicates that the GCC also has great potential in tracking the phenological changes across vegetation types in evergreen forest ecosystems [29–32].

Previous studies have investigated the impact of spatial resolution on vegetation canopy phenology monitoring using multi-scale remote sensing observations. Zhang et al. [33] found that a coarse spatial resolution introduced uncertainties in land surface phenology by comparing phenology derived from coarse and fine resolution imagery; the SOS length obtained using a coarse resolution in a heterogeneous landscape area is almost 40 days less than that obtained using fine resolution. Chen et al. [34] conducted an empirical simulation study and found that considerable phenology extraction uncertainty is associated with coarser spatial resolution and plant species mixing, a finding further confirmed by Liu et al. [35] and Tian et al. [36] using real-world satellite data. Similar mixture effects can be anticipated in tropical forests as spatial resolution changes due to the aggregation of different forest elements (i.e., bare branch, leaf, and shade in our case) within each pixel. This aggregation affects the spectral and spatial information of the pixels [37], resulting in uncertainties in forest phenology characterization. Thapa et al. [38] found agreement between Phenocams, UAVs, and satellite data, which served as a good foundation for analyzing the interoperability of different sensors for vegetation dynamics and change analysis; the regression analysis between time series of NDVI data from different sensors shows high Pearson's correlation coefficients ($r > 0.75$). Similarly, Tran et al. [39] have linked phenological camera data with satellite remote sensing data to generate a new algorithm for gap-free time series of surface phenology. The result indicated that the phenology metrics derived from the algorithm were very close to the observations

from the Phenocam network, with a correlation coefficient of 0.82–0.97, a mean absolute difference of 2.8–3.5 days, and a root mean squared error of 3.5–4.0 days.

Additionally, Phenocams can obtain vegetation phenology at different levels through the selection of ROI. For example, Davidson et al. [40] studied the phenology of different forms of boreal peatland vegetation (defined as bog and fen) at the chamber plot scale (<0.5 $m^2$), while Cheng et al. [41] derived vegetation indices from digital images at the level of individual trees. And, if the distribution of trees in an urban forest is complex and broken, vegetation phenology may respond differently to changes in environmental conditions at different levels, such as warm spells and timing of the growing season's start [42]. However, researchers either focus on the phenological characteristics of urban forests at the landscape scale [43] or on the phenological characteristics of individual trees [44,45], but no researchers have discussed the phenological differences of urban forests at the individual and group levels at the same location. The phenological activities of plants are the result of the combined effects of multiple influencing factors, mainly influenced by external environmental factors, such as temperature, precipitation, sunshine, solar radiation, etc. [46,47]. and also influenced internally by factors like vernalization, photoperiodism, plant growth hormones, enzymes, etc. [48–50].

Therefore, this study, based on Phenocams, obtains high-precision, long-term, and continuous photographic data. Exploring the phenological characteristics of urban forests at a more refined spatial and temporal level plays an important role in optimizing vegetation phenology models. At the same time, refining the research scale to the group or individual level also enables more in-depth study of the changes in key phenological metrics within and among species within the community. Additionally, phenological cameras have been widely used in research across different ecosystems globally for the reliability of their results and their complementarity with remote sensing data at spatiotemporal scales [51], serving as a powerful bridge connecting field observations and remote sensing observations and as a potential tool for addressing the issue of inconsistent scales in phenological research in the future [52,53]. So, our objectives in this study are (1) to extract the phenological changes of *Cinnamomum camphora* and *Bischofia polycarpa* forests from the Phenocam observation data to analyze the variation of phenology; and (2) to compare the differences in vegetation canopy phenological parameters at individual and group levels under a fragmented landscape.

## 2. Materials and Methods

### 2.1. Study Site

The study site is located in suburban Shanghai, southeastern China. The study area has a northern subtropical marine monsoon climate dominated by the southeast wind throughout the year. The average annual rainfall is 1056 mm, the frost-free period is 247 days, and the average temperature is 15.5 °C. The annual average sunshine hours are 1960.7 h, the annual average relative humidity is 82%, the annual average pressure is 1015.4 hPa, and the annual average wind speed is 3.0 m/s. The average annual high-tide water level is 2.71 m, and the low-tide average water level is 2.58 m. The study site is an urban forest consisting of 5–10-year-old mixed artificial planted trees, with the main species including *Cinnamomum camphora*, *Bischofia polycarpa*, *Salix babylonica* L., and *Koelreuteria bipinnata* Laxm. The Phenocam images were acquired using a camera (Campbell Scientific Instruments, Logan, UT, USA) facing north and installed on an eddy flux tower (121°01′ E, 31°08′ N) at a height of 30 m above ground level, pointing north down from the horizontal (Figure 1). The camera captured digital imagery of the foreground canopy within a field of view (FOV) of approximately 550 $m^2$ (Figure 1).

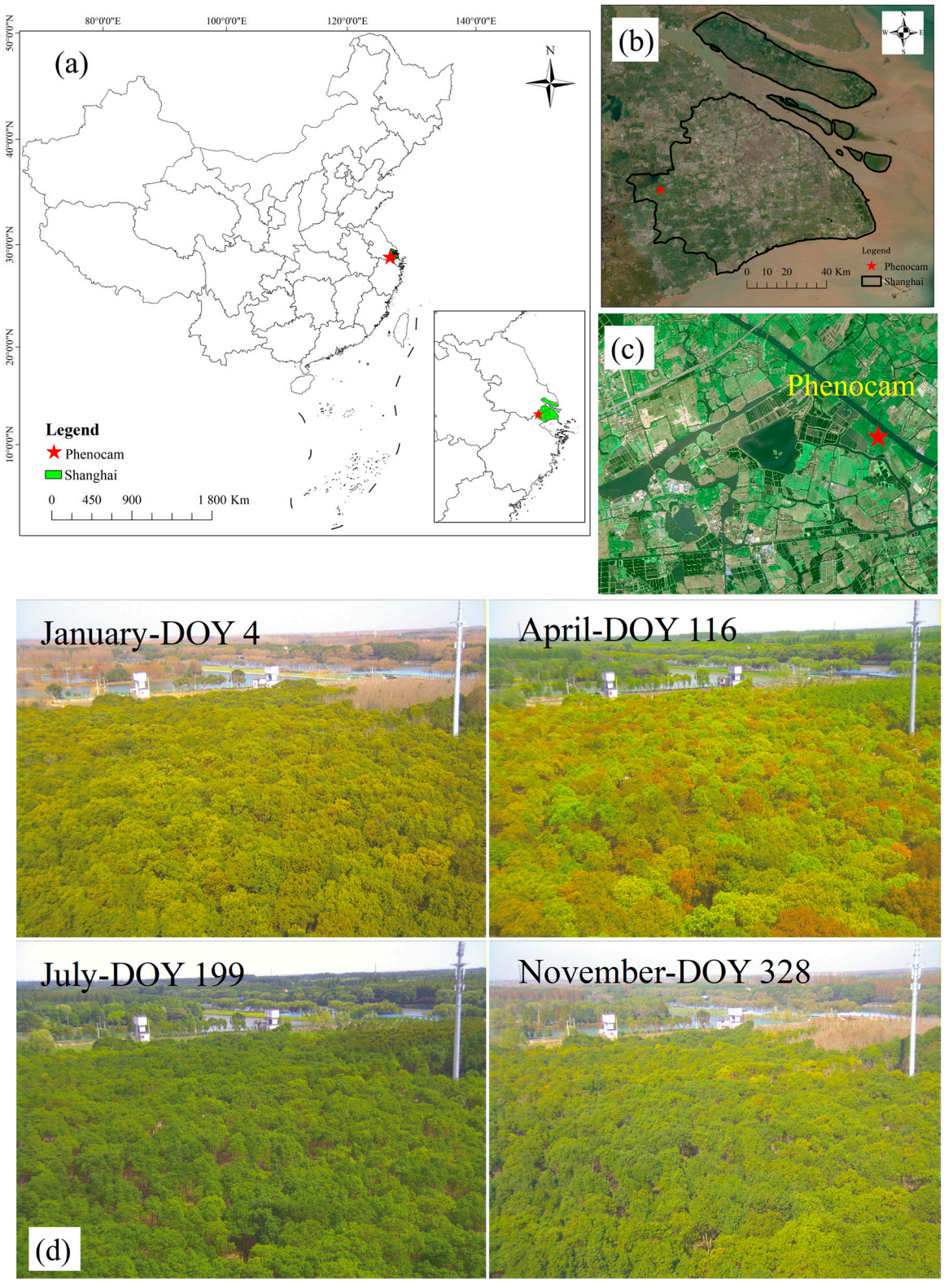


**Figure 1.** (**a**) The location of the study site in China; (**b**) the location of the Phenocam in Shanghai; (**c**) Qingxi Country Park HD image; (**d**) examples of camera photographs.

### *2.2. Phenology Camera Image Pre-Processing*

The camera captured colored three-layer RGB images at an hourly temporal resolution from 5 a.m. to 8 p.m. throughout the year, beginning in January 2021. This study only used images taken between 9 a.m. and 12 p.m. to avoid obtaining images with low solar

elevation, which affects the green chromatic coordinate (GCC) [54]. Subsequently, due to the moderate volume of the data, manual visual screening was performed to screen out the photos that did not meet the lighting requirements or images taken when the lens was dirty and occluded. Removed photos were replaced with the best photos near the same time of the day. The camera images that appeared disoriented, very bright (affected by the solar glare), foggy, or blurred or that had less than 10% visible area were manually removed before the processing procedure. All of the images that passed the quality control filters were used to compute the time series of vegetation indices. A total of 927 photos were selected.

### 2.3. Regions of Interest (ROIs)

Phenopix 3.2.3 (https://cran.r-project.org/web/packages/phenopix/index.html, accessed on 26 June 2021) was designed for processing digital images of the vegetation cover in order to compute vegetation indexes that can in turn be used to track the seasonal development of the vegetation [55]. The package provides functions to process digital images, depict greenness index trajectories, and extract relevant phenological stages. The first step of the work is to set a region of interest on the images; the second step is extracting information from the ROI(s); the third step is data filtering; the fourth step is fitting a curve to the data; and the fifth step is the extraction of phenological thresholds [55,56].

According to the vegetation classification standard, the vegetation in the research area includes *Cinnamomum camphora* and *Bischofia polycarpa* communities. Based on this, we investigated the ability of phenology cameras to capture vegetation phenological characteristics at different vegetation units from the individual and group levels. Specifically, we selected 100 ROIs at the individual level and 4 ROIs at the group level. The positions of the ROIs in the images are shown in Figure 2.

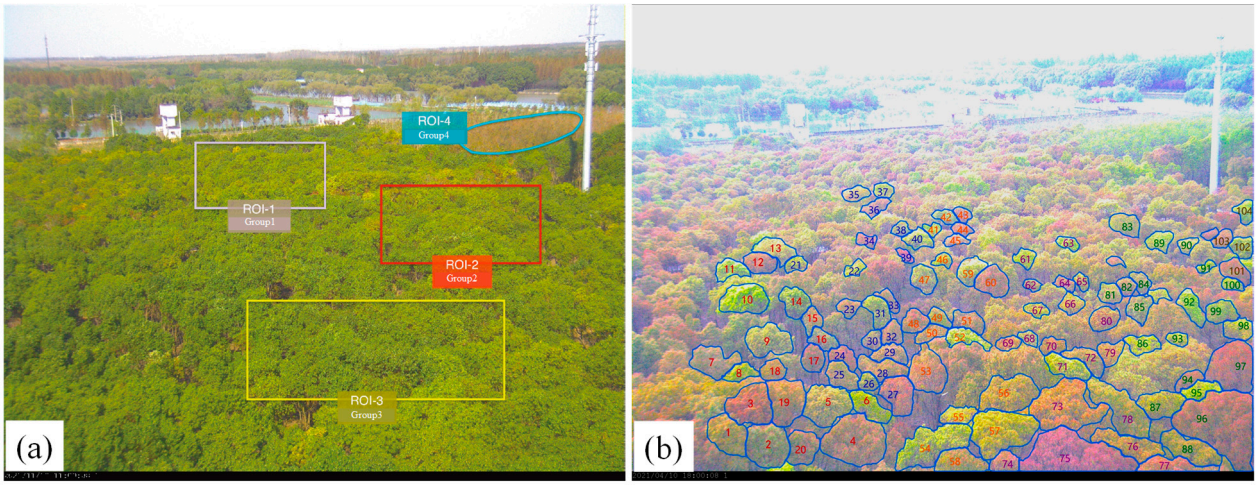


**Figure 2.** Regions of interest (ROIs) 1–3 are the *Cinnamomum camphora* groups, ROI 4 is the *Bischofia polycarpa* group in (**a**), and (**b**) is regions of interest at the individual level.

Through the above division of the ROI, all time series photos were cut according to the contour of the ROI, and the pixel information of the photos in the ROI was extracted to form continuous pixel-value time series data.

### 2.4. Acquisition of the GCC

The vegetation index is a research method used to reflect and measure plants' growth state. Due to its high compatibility with phenological camera technology, the data results are more accurate, and the GCC has become the most widely used vegetation index in near-

surface phenological observation [57]. The GCC was selected as the index to describe the growth state of the urban forest and to simulate the vegetation growth curve (Equation (1)).

$$GCC = \frac{G_{DN}}{R_{DN} + G_{DN} + B_{DN}} \quad (1)$$

In Equation (1), $G_{DN}$, $R_{DN}$, and $B_{DN}$ are the values of green, red, and blue bands in each pixel of the photo interest area, respectively [58]. In the ROI analysis, the range of the GCC is 0.3–0.6.

### 2.5. Data Smoothing and Filtering

The directly acquired photos are inevitably affected by weather and camera imaging principles, and the directly produced data contain noise values. To overcome these issues, filters are applied. There are 5 different filtering approaches implemented in Phenopix, night, blue, mad, spline, and max [55]. Because the images taken at night were not included, the maximum filtering method was selected. The maximum filtering method was used to obtain a sliding window of 3 days as a unit, and the data took the 90th percentile value as the maximum value. For example, a photo was considered to depict a cloudy day when the photo was covered by 90% clouds, with no direct light, while photos with less than 10% cloud cover were defined as photos of the forest canopy with direct sunlight [59]. The maximum value method effectively reduced interference due to the fluctuation of illumination conditions on the stability of the data quality and smoothed the GCC time series without losing important phenological transitions [60]. After filtering all of the data using the maximum value method, they were used as the data basis for the next curve fitting.

### 2.6. Curve Fitting and Phenophase Extraction

The common methods for vegetation growth curve fitting include logistic function fitting, asymmetric Gaussian function fitting, and polynomial fitting [61]. The D-L (Double logistic) method is one of the most widely used plant growth curve fitting methods [62]. The D-L method has been applied to many phenological studies focused on different ecosystems and vegetation types, including a variety of fitting models derived from the D-L method for comparison and selection [55]. In this study, Klosterman's vegetation growth curve fitting model based on the D-L method was selected and applied to different vegetation classification levels to study the applicability of the greenness index extracted using each method for phenological camera photos in simulating the vegetation growth process. The Klosterman method is based on the study of the Elmore method [63] based on the fitting of the fraction of photosynthetic vegetation (FPV) time series. The specific model is shown in Equation (2):

$$F(t) = (a_1 t + b_1) + (a_2 t^2 + b_2 t + c)\left[\frac{1}{[1 + q_1 \exp\ (-\ h_1(t - n_1))]^{v_1}} - \frac{1}{[1 + q_2 \exp(-h_2(t - n_2)]^{v_2}}\right] \quad (2)$$

In Equation (2), $F(t)$ is the modeled value of a vegetation index, such as the GCC, at time $t$. We introduced two additional generalized S-shaped formula parameters ($q_i$ and $v_i$) to the allow different rates of increase near the lower and upper asymptotes of the sigmoid. $a_1$ and $b_1$ control the timing of increase or decrease, and $a_2$ and $b_2$ control the rate of increase or decrease, while $c$ is the amplitude of increase or decrease in greenness [28,64].

After the curve fitting of the vegetation growth trajectory is completed, the key phenological metrics can be extracted based on the fitting curve. In this study, Gu's key phenological parameter extraction method was used. Based on the combination of local maximum values in the first derivative, Gu's method was used to extract the beginning

date of the growth period or the upturn date (UD), the stabilization date (SD) of the growth period, the decline date of the growth period or the downturn date (DD), and the end date of the growth period or the recession date (RD) (Figure 3). The difference between the RD and the UD was the total length of the growth period [65].

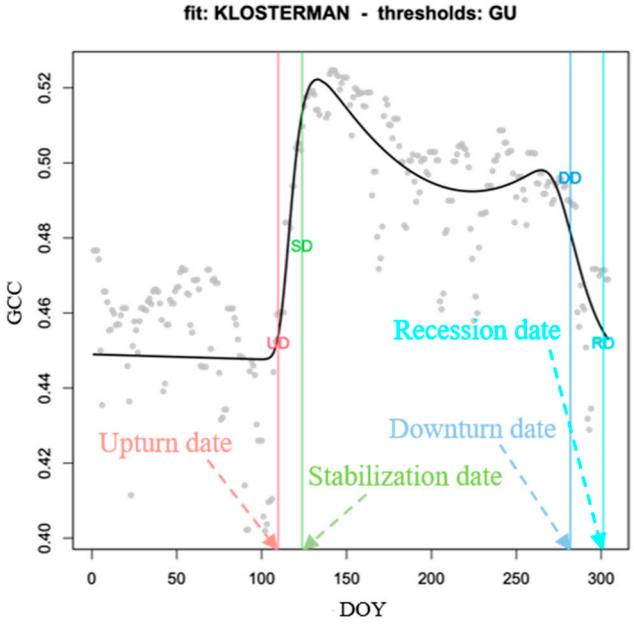


**Figure 3.** Phenological metrics extracted using Klosterman and GU methods.

### 2.7. Statistical Analysis

In order to compare the fitting effect of each fitting method on the vegetation index, the root mean square error (RMSE) between the fitting value and the original vegetation index value was selected for evaluation. The calculation formula is as follows:

$$RMSE = \sqrt{\frac{\sum(VI_i' - VI_i)^2}{n}} \quad (3)$$

where *VIi* is the original vegetation index value for the ith day of year (DOY), $VI_i'$ is the fit value of the day, and *n* is value of the DOY.

When comparing the variation of parameters in different phenological periods, we chose standard deviation (σ) to reflect their differences.

## 3. Results

### 3.1. Comparison of GCC at Different Levels

The GCC time series value at the individual level is the average value of the GCC of each sample. (Figure 4). As shown in Figure 3, the GCC revealed the low period of camphor growth activity in spring and the rising period in April. The trend of the GCC was consistent regardless of the level; the trend decreased slowly in January and then became a gentle upward trend. On the 60th day, the trend of the curve began to decline again, and the fluctuation range increased significantly. This stage continued until the 105th day, when it reached the lowest value in the entire year. After that, the fluctuation range of the curve decreased, but the trend still increased. Between the 105th and the 135th days, the growth rate of the GCC was the greatest in the entire year and the longest positive growth period. This stage corresponded to early April to early May, with the advance of flowering, and the vegetation index reached the lowest value in early May, as camphor flowering came to an end. However, the GCC values at different levels of each accumulated day

showed significant differences. The individual level > the *Cinnamomum camphora* group > the *Bischofia polycarpa* group, which also showed that the more sophisticated the level, the more accurate the description and interpretation of the phenophase. This study also found that the GCC changes between different individuals showed great individual differences and seasonal differences, and the large fluctuations between different individuals exhibited consistency. The group-level GCC was affected by the characteristics of the species growth trajectory and the population size.

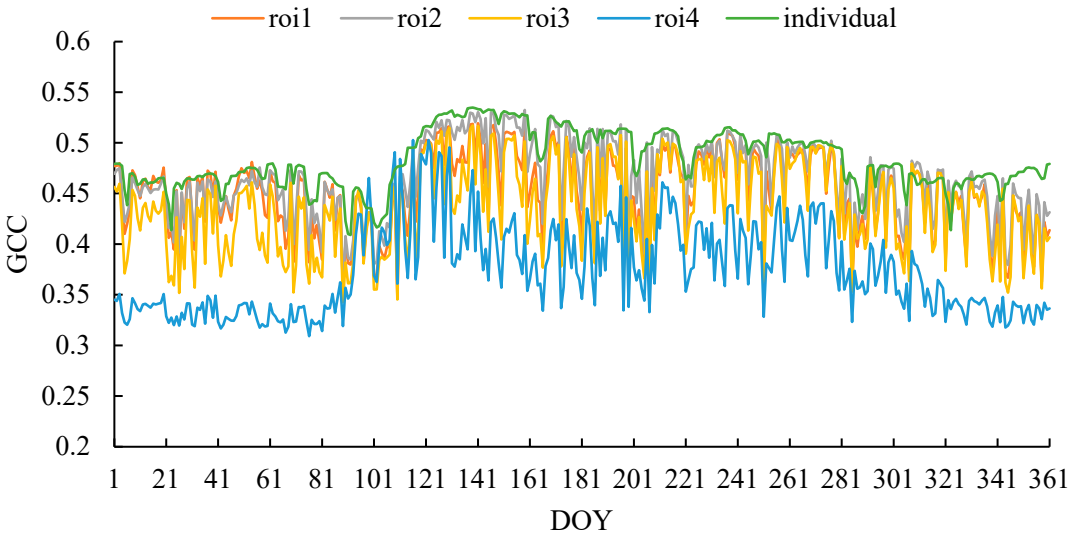


**Figure 4.** Green chromatic coordinate (GCC) time series curves at individual and group levels in an urban forest, where ROIs 1–3 are the *Cinnamomum camphora* groups and ROI 4 is the *Bischofia polycarpa* group.

### *3.2. Key Phenological Metric Extraction Results*

#### 3.2.1. Growth Curve Fitting at the Group Level

The GCC can best describe the difference in the vegetation growth state with seasonal changes and is more suitable for fitting the growth curve than other plant indices. The key phenological period start and end dates and the growth period length were obtained via different phenological metric extraction methods using the fitted growth curve. The Klosterman and Gu phenological metric extraction methods were used to fit the growth curves at the group levels, and the root mean square error (RMSE) value indicated the performance of the model fitting. When Klosterman was used to fit the growth curve of the population in the study area, the peak changes in the plant growth state could be accurately characterized. The RMSE of the *Bischofia polycarpa* group was 0.014, and the RMSEs of the three *Cinnamomum camphora* groups were 0.02, 0.015, and 0.014. The results are shown in Figure 5, in which the red line corresponds to the UD, the green line corresponds to the SD, the blue line corresponds to the DD, and the cyan line corresponds to the RD. The results showed that the Klosterman method could be used to fit the growth curve and the Gu method could be used to extract the phenological metrics of the urban forest (Tables 1 and 2).

**Table 1.** The RMSE of the Klosterman's vegetation growth curve fitting model.

| Level | RMSE |
|---|---|
| *Cinnamomum camphora* population 1 (ROI 1) | 0.02 |
| *Cinnamomum camphora* population 2 (ROI 2) | 0.015 |
| *Cinnamomum camphora* population 3 (ROI 3) | 0.014 |
| *Bischofia polycarpa* population (ROI 4) | 0.014 |

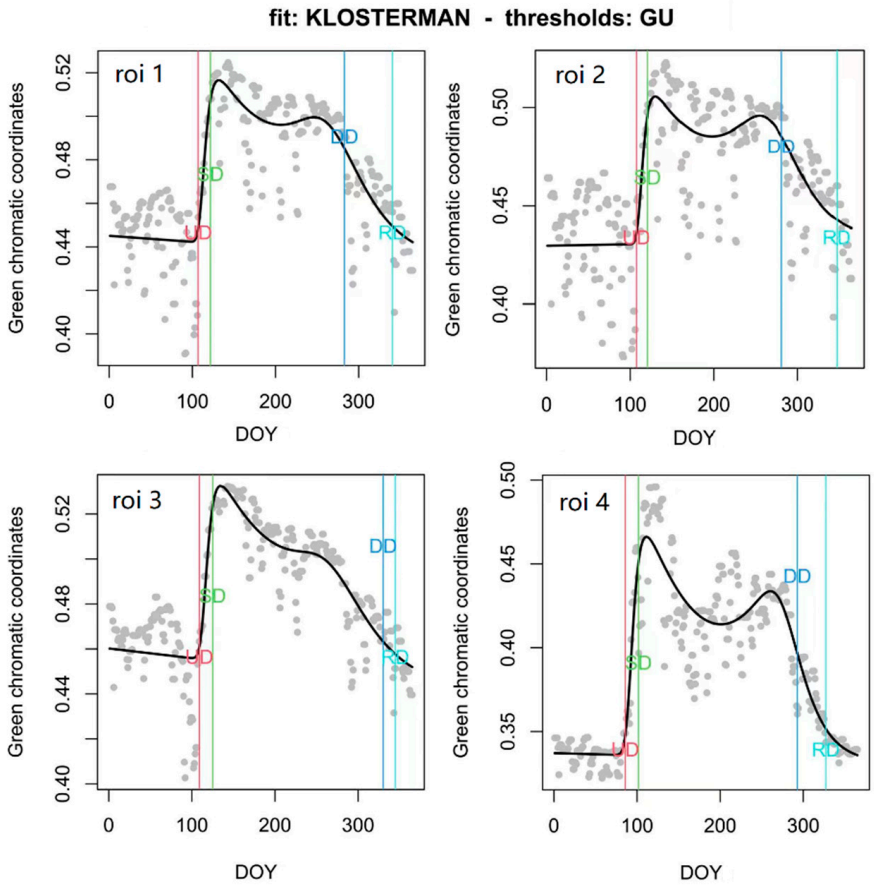


**Figure 5.** Growth curve fitting results, where regions of interest (ROIs) 1–3 are the *Cinnamomum camphora* and ROI 4 is the *Bischofia polycarpa*.

**Table 2.** Extraction results of key phenological metrics at the group level.

| Level | UD | SD | DD | RD | LOS |
|---|---|---|---|---|---|
| *Cinnamomum camphora* group 1 | 110 | 123 | 282 | 292 | 181 |
| *Cinnamomum camphora* group 2 | 106 | 118 | 284 | 295 | 189 |
| *Cinnamomum camphora* group 3 | 108 | 122 | 283 | 293 | 185 |
| *Bischofia polycarpa* group | 86 | 102 | 291 | 318 | 232 |

UD: upturn date, SD: stabilization date, DD: downturn date, RD: recession date, LOS: length of growing season.

### 3.2.2. Key Phenological Metrics at the Group Level

The key phenological metrics included four key date time points and one time length: the UD, the SD, the DD, the RD, and the total length of the growth period (the difference between the RD and the UD).

The phenological metrics of *Cinnamomum camphora* showed high consistency as a whole, and the maximum difference between populations for the same metrics was 4 days. In contrast, there were significant differences in phenological metrics between *Bischofia polycarpa* and *Cinnamomum camphora*. The average growth period of *Cinnamomum camphora* began in late April (around 108th), and their average UD (86th) was 22 days earlier than the average. The SD of the *Cinnamomum camphora* was concentrated from late April to early May (average 121st), which was 19 days later than that of the *Bischofia polycarpa* population (102nd). The RD of *Cinnamomum camphora* showed good consistency, and the difference among the three *Cinnamomum camphora* was 2 or 3 days. The RD of *Bischofia polycarpa* was 8 days ahead of the average. The average growth period of *Cinnamomum camphora* ended in late October (293rd), while the growth period of *Bischofia polycarpa* ended

in mid-November, with an average difference of 25 days. The growth period of *Bischofia polycarpa* was significantly longer than that of *Cinnamomum camphora*, with an average of 47 days.

Figure 6 intuitively shows the differences in phenological metrics between different species. *Bischofia polycarpa* entered the growth period earlier, and the time required to reach the SD was not much different from that of *Cinnamomum camphora*. The stable stage during the growth period was slightly longer than that of *Cinnamomum camphora*, and the period from the DD to the RD was longer. The total growth period was significantly longer than that of *Cinnamomum camphora*.

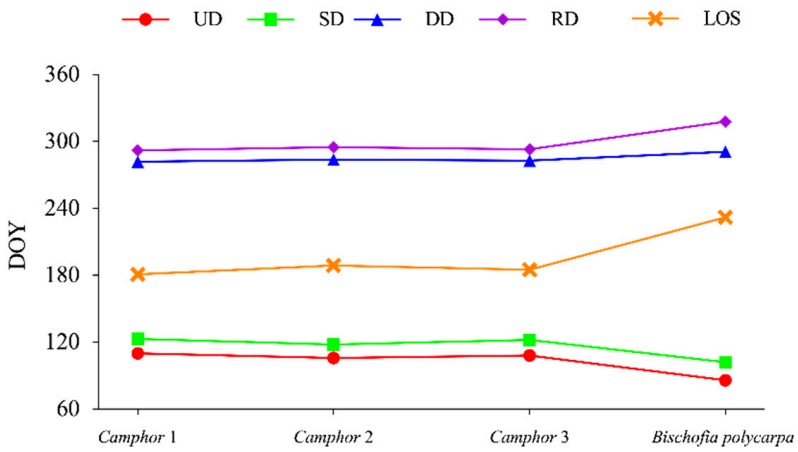


**Figure 6.** Comparison of key phenological metrics at the population level.

The differences in phenological metrics between *Cinnamomum camphora* and *Bischofia polycarpa* corresponded to the change trend of the vegetation index. Figure 7 combines the mean values of the phenological metrics of the three *Cinnamomum camphora* groups, the phenological metrics of the *Bischofia polycarpa*, and the GCC time series curves of the two. From January to March, the relative greenness index of the *Cinnamomum camphora* and the *Bischofia polycarpa* did not change significantly, and there was a relatively stable difference between them of about 0.1. The peak of the GCC in *Cinnamomum camphora* appeared later than that in *Bischofia polycarpa*, which was consistent with the difference in the UD. Observing only the GCC curve, the difference between the UD and the SD of the growth period was obvious, but the DD and the RD were blurred, and the length seemed to be not much different. The extraction of phenological metrics revealed that the two species exhibited great differences in the characteristics of the late growth period. As an evergreen broad-leaved forest, the GCC value of *Cinnamomum camphora* was high, and it was difficult to see the real growth change rate based on its change trend in the middle and late growth periods. By combining the GCC curve and the key time points of the phenological process, the actual and more accurate growth state change dynamics of *Cinnamomum camphora* were obtained. The dynamic curve of the growth state of the *Bischofia polycarpa* showed that its change trend was significantly different from the curve of the *Cinnamomum camphora*. Throughout the year, the *Bischofia polycarpa* was dormant from January to February and showed an obvious growth peak from March to early May, with the highest value in early May. The GCC of *Cinnamomum camphora* peaked from mid-May to July, after which it remained flat at a medium level, before continuing to decline until the end of the year in September.

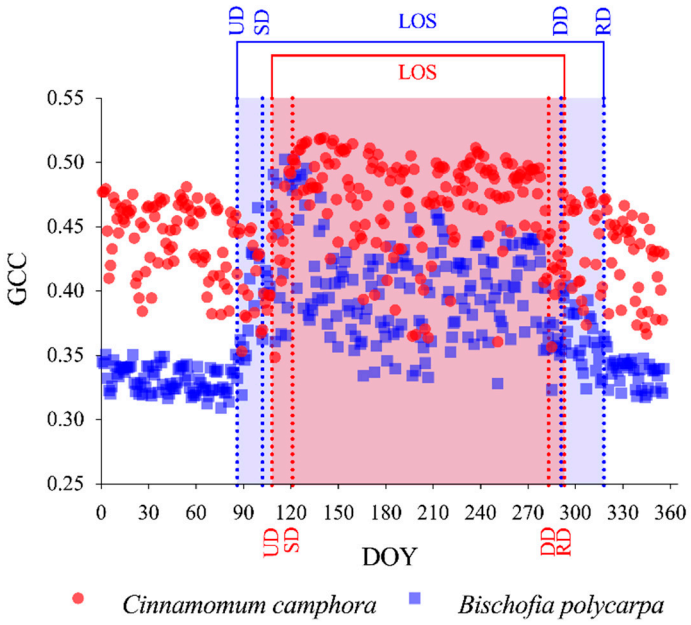


**Figure 7.** Green chromatic coordinate (GCC) curves and key phenological metrics of *Cinnamomum camphora* and *Bischofia polycarpa*.

### 3.2.3. Key Phenological Metrics of Individuals

Figure 8 shows the key phenological metrics of urban forest camphor at the individual level. The greatest difference in phenological metrics between different individuals was the length of the growth period, with a maximum difference of 106 days. There was no obvious causal relationship between the UD and the RD of the growth period and the length of the growth period, and the uncertainty was high. Among the four growth period time point metrics, the UD ($\sigma$ = 8) and the SD ($\sigma$ = 5) had the least significant difference among individuals within the species, and the DD ($\sigma$ = 45) had the largest difference. Among 44 individuals of *Cinnamomum camphora*, the DDs of four individuals (Nos. 30, 33, 36, and 44) showed a very low value; the length of their stable growth period was significantly shorter, and they entered the decline stage of the growth period earlier.

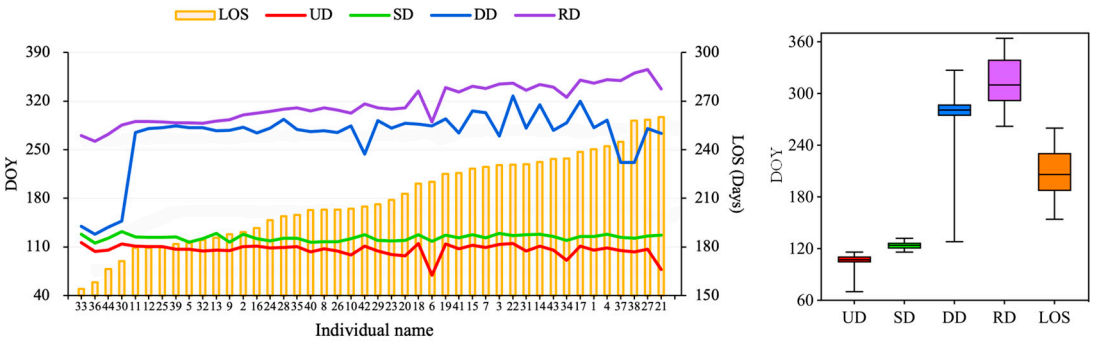


**Figure 8.** Individual key phenological metrics of *Cinnamomum camphora*; the positions of box plots represent the 5th, 25th, 50th, 75th, and 95th percentiles, respectively.

### *3.3. Comparison of Key Phenological Metrics at Different Levels*

The DD appeared last, the RD was the earliest, and the LOS was the smallest (185 d) in *Cinnamomum camphora* groups. The group-level growth period of *Cinnamomum camphora* ended the earliest at 42 days earlier than the individual level, and the total growth period was the shortest (185 d) at 44 days less than the individual level. The difference between individuals and groups was the largest, and the change between *Cinnamomum camphora*

groups was not obvious. The individual level showed the most diverse results, with the longest stage between aging and dormancy (42 d) and the longest growth length (209 d). The changes in the UD and the SD were the smallest, within 1–3 days between individual and group levels (Figure 9).

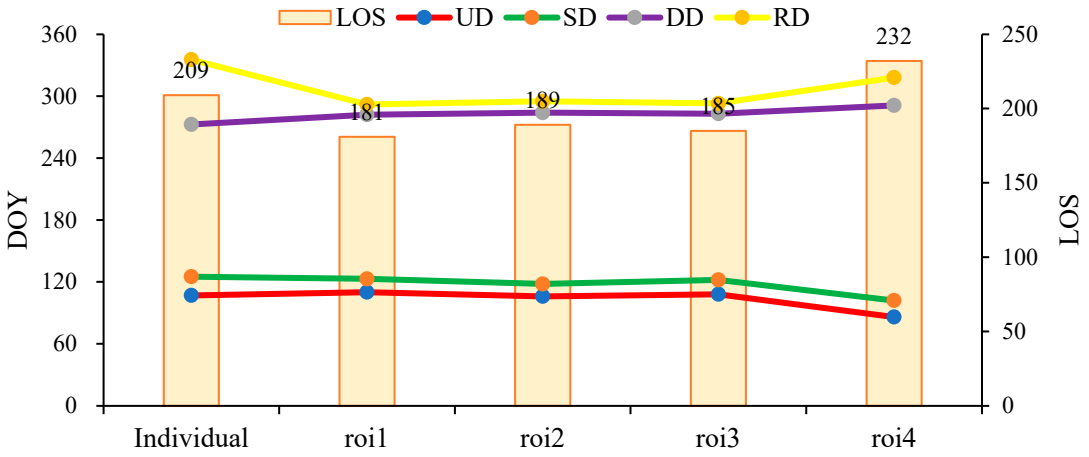


**Figure 9.** Comparison of key phenological metrics at three different levels; the boxes with numbers in it represent the LOS. ROIs 1–3 are *Cinnamomum camphora*; ROI 4 is *Bischofia polycarpa*.

## 4. Discussion

The GCC showed a change in the vegetation growth state (Figure 4) that indicated green-up and senescence processes at individual and group levels in the urban forest. Furthermore, these results are in agreement with the work on forests of other authors [29,38,66]. This conclusion depends on the homogenous vegetation distribution type in the study area, a single species, and similar tree ages. There were large differences between the individual level and the group level. One of the possible explanations is that there were inevitably canopy gaps in the community and population interest areas, that is, understory areas with low vegetation coverage and low biomass. According to the principle of GCC calculation, such regions will lead to an increase in the GCC denominator, which weakens the change of the green pixel color value as a numerator. This is similar to the principle that coarser spatial resolution could lead to greater uncertainty in phenology monitoring, as the pixel size grows as the species mixture increases, which reduces the probability of pure pixels in coarser-resolution images [67,68]. The individual-level ROI only included the canopy area, and the interference value was less when calculating the vegetation index. In our study, we found that four trees had significantly different phenological metrics from other individuals. We located the four trees and found that they all had small DBH (Diameter at Breast Height) and survived in low-lying areas. We believe that due to the physiological characteristics and living environment of these four trees, they show obvious phenological differences from other trees. Some research has shown that individual tree crowns are fundamental components of the upper canopy plant community, and their seasonal variations in deciduousness collectively influence critical ecosystem processes, including photosynthetic seasonality, hydrological regulation, and nutrient cycling [69,70]. Ecologically, variations in phenological patterns could be correlated with the adaptive responses of individual trees to abiotic environments, such as ground water storage, soil fertility, or microclimates [60,71], and biotic processes, such as adjustments in leaf emergence and shedding timing, to mitigate intraspecific and interspecific competitions [72,73] or to reduce herbivore predation and pathogen infection on young leaves [74]. The GCC has very high accuracy for the extraction of vegetation phenological information. Thapa et al. [38] compared the potential of NDVI, the GCC, and the VIgreen index to represent

vegetation phenology based on different near-ground vegetation observation methods. The results showed that the GCC was the recommended VI for characterizing phenology phases and transition dates; the same result was obtained by Alberton et al. [60]. There are great differences in phenological characteristics among different populations. Although the population of *Bischofia polycarpa* was deciduous, its growing period length was longer than that of evergreen species, and the UD of *Bischofia polycarpa* is earlier than that of *Cinnamomum camphora*, which was similar to the results obtained by Ide and Oguma [75] for green-up dates for different populations in Japanese national parks.

Although the photos obtained based on the phenological camera contain data that can accurately reflect the growth dynamics and phenological characteristics of vegetation, the correct selection of the key phenological metrics of vegetation directly affects the phenological characteristics of vegetation. The Beck method [62], the Gu method [65], the Elmore method [63], and the Klosterman method [28] are commonly used to fit growth curve. In this paper, we used the Klosterman method to fit the growth curve and the Gu method was used to extract the phenological period, and the results were consistent with the conclusions obtained by Richardson et al. [27] in their study of temperate forest ecosystems in North America. TIMESAT 3.2 software [76] was also used to extract phenological events: the start of the season (SOS), the maximum of the season (MOS), and the end of the season (EOS). In addition, the regional Phenocam had no standardized white reflectance panel for reference when taking photos. Through a literature search, we found that many similar studies did not have a standardized white reflectance panel [51,66,77]. The study by Petach et al. [78] also verified that high-quality canopy vegetation index data can be obtained even without a white reflectance panel.

At different research levels, the pixel values of the original photos did not change, and the results of phenological metrics produced level regularity. In this paper, the individual phenological information extraction of an urban forest with a small spatial range and low spatial heterogeneity was performed. The method of interest area division used was highly dependent on the conditions of a neat individual position and a similar canopy area for the trees in the study area. How to extract multi-species phenological information in other forest ecosystems with complex natural conditions is a research direction that can be further investigated in future work. Under the increasing pace of urbanization and rapidly changing urban ecosystems, the extraction of large-level phenological information has been unable to meet the monitoring requirements for the fragmentation and patchy distribution of vegetation blocks produced during urbanization [79,80], and more accurate acquisition of vegetation growth status and phenological information is required [81]. Scattered native vegetation and artificial vegetation patches in urban ecosystems are among the ecosystem components affected the most directly by urbanization and human activities, and they are the ecological indicators that respond the most quickly to urban environmental changes [82]. How to clarify the correlation and interaction mechanism of species and interspecific phenological information on a small scale may be a feasible way to monitor and manage vegetation, ecosystems, and human activities in the process of urbanization [83]. If complete phenological information can be accurately captured without the restriction of spatial scale, phenological information in space and time will be further expanded so that the conclusion does not depend on the research scale [84]. Therefore, the extraction of vegetation phenology at different scales will be explored in future research. From the LSP at the vast spatial scale to the intraspecific and interspecific relationships of individual phenology, how to quantitatively connect the results of research conducted at different scales based on the relationships between ecological activities will be a problem to be solved in the future [85].

Urbanization is an important factor affecting the phenology of urban vegetation [43,86]. With the acceleration of the urbanization process, people are paying more attention to the health and function of vegetation in cities. Due to the urban heat island effect, vegetation in urban areas always has a longer growing season than vegetation in suburban areas [87,88]. However, research on urban forest phenology is always limited by temporal or spatial resolution. While MODIS data can provide a long time series of vegetation index data and phenology products, their spatial resolution is relatively coarse [86]; although PlanetScope and Sentinel-2 have improved spatial resolution to the meter level, their temporal resolution is not ideal [87]. This study used Phenocam for long-term continuous monitoring of urban forest phenology, with a temporal resolution of hours and a spatial resolution at the meter level, and it is not affected by clouds [75,77]. Based on the results of this study, by comparing the phenological characteristics of vegetation in different individuals, we can identify abnormal plants and even understand whether it is due to diseases or pests [89,90] or pay attention to germination or flowering [77,91]. Monitoring the phenological changes of vegetation in different groups can help us deeply study the growth and development patterns of different vegetation under different environmental conditions, providing a scientific basis for monitoring and predicting the growth status of vegetation [92]. Therefore, conducting phenological monitoring of urban forests at different levels can not only refine urban greening management, accurately grasping the health status of each tree, but also provide support for decision making in regional ecosystem management, resource protection, and environmental monitoring.

## 5. Conclusions

Using the phenological camera, this study collected photos during 2021, calculated the vegetation index, and extracted the phenological metrics. The phenological metrics of the forest canopy were extracted at different research levels, and the results were highly consistent. The GCC gave a specific and accurate description of the growth status of vegetation and was suitable for the evergreen broad-leaved tree species *Cinnamomum camphora* and the deciduous tree species *Bischofia polycarpa*. The phenological metrics extracted using the Klosterman and Gu models reflected the phenology trend of the urban forest canopy. According to the analysis of the results, we draw the following conclusions. (1) The results of the three groups of *Cinnamomum camphora* were basically the same, while the phenological characteristics of the *Cinnamomum camphora* and *Bischofia polycarpa* groups were significantly different. *Bischofia polycarpa* had a longer growth period (average difference of 47 days), the growth period started 22 days earlier, and the weak point of the growth period was 25 days later. (2) The LOS of *Cinnamomum camphora* at the individual level was 24 days longer than that at the group level. Although the results in this paper could more accurately reflect the phenological characteristics of an urban forest canopy at different levels, only one point was selected in this paper, and the time span was only one year. The characteristics of urban microclimates are remarkable. Therefore, it is necessary to study the long-term variation of urban forest phenology at different locations in the city in the future. Meanwhile, quantifying the influencing factors of urban forest phenology under different environmental backgrounds is also a very interesting topic. These studies are crucial for more comprehensively understanding and grasping the dynamic characteristics of vegetation phenology in the fragmented urban landscape.

**Author Contributions:** Conceptualization, K.Z. and J.G.; Methodology, K.Z. and J.G.; Software, J.B.; Formal analysis, K.Z.; Investigation, K.Z. and J.B.; Resources, K.Z.; Data curation, J.B.; Writing—original draft, K.Z.; Visualization, J.B.; Supervision, J.G.; Project administration, J.G.; Funding acquisition, J.G. All authors have read and agreed to the published version of the manuscript.

**Funding:** This work was supported by a grant from the Joint Research Project for Meteorological Capacity Improvement (Grant No. 22NLTSQ011) and the Key Program of the National Natural Science Foundation of China (Grant No. 41730642).

**Data Availability Statement:** The data are available from the corresponding author upon reasonable request.

**Acknowledgments:** We greatly appreciate the suggestions for illuminating the manuscript given by the anonymous reviewers, and thanks also to the editorial staff.

**Conflicts of Interest:** The authors declare no competing financial interests.

## References

1. Bruyninckx, H.H.D.; Hellweg, S.; Schandl, S.; Vidal, H.; Razian, B.; Nohl, H.; Christopher Pfister, S. *Global Resources Outlook 2024: Bend the Trend-Pathways to a Liveable Planet as Resource Use Spikes*; United Nations Environment Programme: Nairobi, Kenya, 2024.
2. Liu, Z.; He, C.; Zhou, Y.; Wu, J. How much of the world's land has been urbanized, really? A hierarchical framework for avoiding confusion. *Landsc. Ecol.* **2014**, *29*, 763–771. [CrossRef]
3. United Nations. *World Urbanization Prospects: The 2018 Revision*; United Nations: New York, NY, USA, 2019.
4. Zipper, S.; Schatz, J.; Singh, A.; Kucharik, C.; Townsend, P.; Loheide, S. Urban heat island impacts on plant phenology: Intra-urban variability and response to land cover. *Environ. Res. Lett.* **2016**, *11*, 054023. [CrossRef]
5. Lieth, H. (Ed.) *Phenology and Seasonality Modeling*; Springer: Berlin/Heidelberg, Germany, 1974; Volume 8.
6. Joiner, J.; Yoshida, Y.; Zhang, Y.; Duveiller, G.; Jung, M.; Lyapustin, A.; Wang, Y.; Tucker, C. Estimation of terrestrial global gross primary production (GPP) with satellite data-driven models and eddy covariance flux data. *Remote Sens.* **2018**, *10*, 1346. [CrossRef]
7. Piao, S.; Liu, Q.; Chen, A.; Janssens, I.A.; Fu, Y.; Dai, J.; Liu, L.; Lian, X.; Shen, M.; Zhu, X. Plant phenology and global climate change: Current progresses and challenges. *Glob. Change Biol.* **2019**, *25*, 1922–1940. [CrossRef]
8. Zhang, Q.; Kong, D.; Shi, P.; Singh, V.P.; Sun, P. Vegetation phenology on the Qinghai-Tibetan Plateau and its response to climate change (1982–2013). *Agric. For. Meteorol.* **2018**, *248*, 408–417. [CrossRef]
9. Escobedo, F.J.; Kroeger, T.; Wagner, J.E. Urban forests and pollution mitigation: Analyzing ecosystem services and disservices. *Environ. Pollut.* **2011**, *159*, 2078–2087. [CrossRef]
10. Li, X.; Zhou, Y.; Meng, L.; Asrar, G.R.; Lu, C.; Wu, Q. A dataset of 30 m annual vegetation phenology indicators (1985–2015) in urban areas of the conterminous United States. *Earth Syst. Sci. Data* **2019**, *11*, 881–894. [CrossRef]
11. Mura, C.; Butt'o, V.; Silvestro, R.; Deslauriers, A.; Charrier, G.; Raymond, P.; Rossi, S. The early bud gets the cold: Diverging spring phenology drives exposure to late frost in a *Picea mariana* [(mill.) BSP] common garden. *Physiol. Plant* **2022**, *174*, e13798. [CrossRef]
12. Jiang, J.; Johansen, K.; Tu, Y.H.; McCabe, M.F. Multi-sensor and multi-platform consistency and interoperability between UAV, planet CubeSat, Sentinel-2, and Landsat reflectance data. *GISci. Remote Sens.* **2022**, *59*, 936–958. [CrossRef]
13. Dai, J.; Zhu, M.; Mao, W.; Liu, R.; Wang, H.; Alatalo, J.M.; Tao, Z.; Ge, Q. Divergent changes of the elevational synchronicity in vegetation spring phenology in North China from 2001 to 2017 in connection with variations in chilling. *Int. J. Climatol.* **2021**, *41*, 6109–6121. [CrossRef]
14. Ding, X.; Jiang, Y.; Xue, F.; Zhang, Y.; Wang, M.; Kang, M.; Xu, H. Intra-annual growth dynamics of *Picea meyeri* needles, shoots, and stems on Luya Mountain, north-Central China. *Trees* **2021**, *35*, 637–648. [CrossRef]
15. Vitasse, Y.; Signarbieux, C.; Fu, Y.H. Global warming leads to more uniform spring phenology across elevations. *Proc. Natl. Acad. Sci. USA* **2018**, *115*, 1004–1008. [CrossRef] [PubMed]
16. Tal, O. Flowering phenological pattern in crowns of four temperate deciduous tree species and its reproductive implications. *Plant Biol.* **2011**, *13*, 62–70. [CrossRef] [PubMed]
17. Wang, J.; Song, G.; Liddell, M.; Morellato, P.; Lee, C.K.; Yang, D.; Alberton, B.; Detto, M.; Ma, X.; Zhao, Y.; et al. An ecologically-constrained deep learning model for tropical leaf phenology monitoring using PlanetScope satellites. *Remote Sens. Environ.* **2023**, *286*, 113429. [CrossRef]
18. Guo, Y.; Chen, S.; Fu, Y.; Xiao, Y.; Wu, W.; Wang, H.; Beurs, K. Comparison of Multi-Methods for Identifying Maize Phenology Using PhenoCams. *Remote Sens.* **2022**, *14*, 244. [CrossRef]
19. Gao, F.; Anderson, M.C.; Zhang, X.; Yang, Z.; Alfieri, J.G.; Kustas, W.P.; Mueller, R.; Johnson, D.M.; Prueger, J.H. Toward mapping crop progress at field scales through fusion of Landsat and MODIS imagery. *Remote Sens. Environ.* **2017**, *188*, 9–25. [CrossRef]
20. Borgogno-Mondino, E.; Fissore, V. Reading Greenness in Urban Areas: Possible Roles of Phenological Metrics from the Copernicus HR-VPP Dataset. *Remote Sens.* **2022**, *14*, 4517. [CrossRef]

21. Fawcett, D.; Bennie, J.; Anderson, K. Monitoring spring phenology of individual tree crowns using drone-acquired NDVI data. *Remote Sens. Ecol. Conserv.* **2021**, *7*, 227–244. [CrossRef]
22. Kabiri, K. Mapping coastal ecosystems and features using a low-cost standard drone: Case study, Nayband Bay, Persian gulf, Iran. *J. Coast. Conserv.* **2020**, *24*, 62. [CrossRef]
23. Assmann, J.J.; Myers-Smith, I.H.; Kerby, J.T.; Cunliffe, A.M.; Daskalova, G.N. Drone data reveal heterogeneity in tundra greenness and phenology not captured by satellites. *Environ. Res. Lett.* **2020**, *15*, 125002. [CrossRef]
24. Wu, S.; Wang, J.; Yan, Z.; Song, G.; Wu, J. Monitoring tree-crown scale autumn leaf phenology in a temperate forest with an integration of planetscope and drone remote sensing observations. *ISPRS J. Photogramm. Remote Sens.* **2021**, *171*, 36–48. [CrossRef]
25. Zhang, S.; Butt'o, V.; Khare, S.; Deslauriers, A.; Morin, H.; Huang, J.-G.; Ren, H.; Rossi, S. Calibrating PhenoCam data with phenological observations of a black spruce stand. *Can. J. Remote. Sens.* **2020**, *46*, 154–165. [CrossRef]
26. Melaas, E.K.; Sulla-Menashe, D.; Gray, J.M.; Black, T.A.; Morin, T.H.; Richardson, A.D.; Friedl, M.A. Multisite analysis of land surface phenology in north American temperate and boreal deciduous forests from Landsat. *Remote Sens. Environ.* **2016**, *186*, 452–464. [CrossRef]
27. Richardson, A.; Hufkens, K.; Milliman, T.; Frolking, S. Intercomparison of phenological transition dates derived from the PhenoCam Dataset V1.0 and MODIS satellite remote sensing. *Sci. Rep.* **2018**, *8*, 5679. [CrossRef] [PubMed]
28. Klosterman, S.T.; Hufkens, K.; Gray, J.M.; Melaas, E.; Sonnentag, O.; Lavine, I.; Mitchell, L.; Norman, R.; Friedl, M.A.; Richardson, A.D. Evaluating remote sensing of deciduous forest phenology at multiple spatial scales using PhenoCam imagery. *Biogeosciences* **2014**, *11*, 4305–4320. [CrossRef]
29. Li, X.; Khare, S.; Khare, S.; Jiang, N.; Liang, E.; Deslauriers, A.; Rossi, S. Comparing phenocam color indices with phenological observations of black spruce in the boreal forest. *Ecol. Inform.* **2023**, *76*, 102149. [CrossRef]
30. Zhou, X.; Wang, X.; Zhang, S.; Zhang, Y.; Bai, X. Combining phenological camera photos and modis reflectance data to predict GPP daily dynamics for alpine meadows on the tibetan plateau. *Remote Sens.* **2020**, *12*, 3735. [CrossRef]
31. Snyder, K. Changes in meadow phenology in response to grazing management at multiple scales of measurement. *Remote Sens.* **2021**, *13*, 4028. [CrossRef]
32. Xie, Y.; Wilson, A. Change point estimation of deciduous forest land surface phenology. *Remote Sens. Environ.* **2020**, *240*, 111698. [CrossRef]
33. Zhang, X.; Wang, J.; Gao, F.; Liu, Y.; Schaaf, C.; Friedl, M.; Yu, Y.; Jayavelu, S.; Gray, J.; Liu, L.; et al. Exploration of scaling effects on coarse resolution land surface phenology. *Remote Sens. Environ.* **2017**, *190*, 318–330. [CrossRef]
34. Chen, X.; Wang, D.; Chen, J.; Wang, C.; Shen, M. The mixed pixel effect in land surface phenology: A simulation study. *Remote Sens. Environ.* **2018**, *211*, 338–344. [CrossRef]
35. Liu, L.; Cao, R.; Shen, M.; Chen, J.; Wang, J.; Zhang, X. How does scale effect influence spring vegetation phenology estimated from satellite-derived vegetation indexes? *Remote Sens.* **2019**, *11*, 2137. [CrossRef]
36. Tian, J.; Zhu, X.; Wu, J.; Shen, M.; Chen, J. Coarse-Resolution Satellite Images Overestimate Urbanization Effects on Vegetation Spring Phenology. *Remote Sens.* **2020**, *12*, 117. [CrossRef]
37. Chen, W.; Henebry, G.M. Change of spatial information under rescaling: A case study using multi-resolution image series. *ISPRS J. Photogramm. Remote Sens.* **2009**, *64*, 592–597. [CrossRef]
38. Thapa, S.; Garcia Millan, V.; Eklundh, L. Assessing Forest Phenology: A Multi-Scale Comparison of Near-Surface (UAV, Spectral Reflectance Sensor, PhenoCam) and Satellite (MODIS, Sentinel-2) Remote Sensing. *Remote Sens.* **2021**, *13*, 1597. [CrossRef]
39. Tran, K.H.; Zhang, X.; Ketchpaw, A.R.; Wang, J.; Ye, Y.; Shen, Y. A novel algorithm for the generation of gap-free time series by fusing harmonized Landsat 8 and Sentinel-2 observations with PhenoCam time series for detecting land surface phenology. *Remote Sens. Environ.* **2022**, *282*, 113275. [CrossRef]
40. Davidson, S.J.; Goud, E.M.; Malhotra, A.; Estey, C.O.; Korsah, P.; Strack, M. Linear disturbances shift boreal peatland plant communities toward earlier peak greenness. *J. Geophys. Res. Biogeosciences* **2021**, *126*, e2021JG006403. [CrossRef]
41. Cheng, Y.; Vrieling, A.; Fava, F.; Meroni, M.; Marshall, M.; Gachoki, S. Phenology of short vegetation cycles in a Kenyan rangeland from PlanetScope and Sentinel-2. *Remote Sens. Environ.* **2020**, *248*, 112004. [CrossRef]
42. Linkosalmi, M.; Tuovinen, J.-P.; Nevalainen, O.; Peltoniemi, M.; Taniş, C.M.; Arslan, A.N.; Aurela, M. Tracking vegetation phenology of pristine northern boreal peatlands by combining digital photography with $CO_2$ flux and remote sensing data. *Biogeosciences* **2022**, *19*, 4747–4765. [CrossRef]
43. Hu, M.; Li, X.; Xu, Y.; Huang, Z.; Chen, C.; Chen, J.; Du, H. Remote sensing monitoring of the spatiotemporal dynamics of urban forest phenology and its response to climate and urbanization. *Urban Clim.* **2024**, *53*, 101810. [CrossRef]
44. Abbas, S.; Peng, Q.; Wong, M.S.; Li, Z.; Hui, K.K.W. Characterizing and classifying urban tree species using bi-monthly terrestrial hyperspectral images in Hong Kong. *ISPRS J. Photogramm. Remote Sens.* **2021**, *177*, 204–216. [CrossRef]
45. Alonzo, M.; Baker, M.E.; Caplan, J.S.; Williams, A.; Elmore, A.J. Canopy composition drives variability in urban growing season length more than the heat island effect. *Sci. Total Environ.* **2023**, *884*, 163818. [CrossRef] [PubMed]

46. Gómez-Giráldez, P.J.; Pérez-Palazón, M.J.; Polo, M.J.; González-Dugo, M.P. Monitoring grass phenology and hydrological dynamics of an oak–grass savanna ecosystem using Sentinel-2 and terrestrial photography. *Remote Sens.* **2020**, *12*, 600. [CrossRef]
47. Nandy, S.; Ghosh, S.; Singh, S. Assessment of sal (*Shorea robusta*) forest phenology and its response to climatic variables in India. *Environ. Monit. Assess.* **2021**, *193*, 616. [CrossRef] [PubMed]
48. Atkins, J.W.; Stovall, A.; Yang, X. Mapping temperate forest phenology using tower, UAV, and terrestrial-based sensors. *Drones* **2020**, *4*, 56. [CrossRef]
49. Lim, C.H.; An, J.H.; Jung, S.H.; Nam, G.B.; Cho, Y.C.; Kim, N.S.; Lee, C.S. Ecological consideration for several methodologies to diagnose vegetation phenology. *Ecol. Res.* **2018**, *33*, 363–377. [CrossRef]
50. St Peter, J.; Hogland, J.; Hebblewhite, M.; Hurley, M.; Hupp, N.; Proffitt, K. Linking phenological indices from digital cameras in Idaho and Montana to MODIS NDVI. *Remote Sens.* **2018**, *10*, 1612. [CrossRef]
51. Burke, M.; Rundquist, B. Scaling phenocam GCC, NDVI, and EVI2 with harmonized Landsat-Sentinel using gaussian processes. *Agric. For. Meteorol.* **2021**, *300*, 108316. [CrossRef]
52. Yan, D.; Zhang, X.; Nagai, S.; Yu, Y.; Akitsu, T.; Nasahara, K.N.; Maeda, T. Evaluating land surface phenology from the Advanced Himawari Imager using observations from MODIS and the Phenological Eyes Network. *Int. J. Appl. Earth Obs. Geoinf.* **2019**, *79*, 71–83. [CrossRef]
53. Watson, C.; Restrepo-Coupe, N.; Huete, A. Multi-Scale phenology of temperate grasslands: Improving monitoring and management with near-surface phenocams. *Front. Environ. Sci.* **2019**, *7*, 14. [CrossRef]
54. Jorge, C.; Silva, J.; Boavida-Portugal, J.; Soares, C.; Cerasoli, S. Using digital photography to track understory phenology in Mediterranean Cork Oak Woodlands. *Remote Sens.* **2021**, *13*, 776. [CrossRef]
55. Filippa, G.; Cremonese, E.; Migliavacca, M.; Galvagno, M.; Forkel, M.; Wingate, L.; Richardson, A.D. Phenopix: AR package for image-based vegetation phenology. *Agric. For. Meteorol.* **2016**, *220*, 141–150. [CrossRef]
56. Knox, S.; Dronova, I.; Sturtevant, C.; Oikawa, P.; Matthes, J.; Verfaillie, J.; Baldocchi, D. Using digital camera and Landsat imagery with eddy covariance data to model gross primary production in restored wetlands. *Agric. For. Meteorol.* **2017**, *237–238*, 233–245. [CrossRef]
57. Norris, J.; Walker, J. Solar and sensor geometry, not vegetation response, drive satellite NDVI phenology in widespread ecosystems of the western United States. *Remote Sens. Environ.* **2020**, *249*, 112013. [CrossRef]
58. Ao, Z.; Sun, Y.; Xin, Q. Constructing 10-m NDVI time series from Landsat 8 and Sentinel 2 images using convolutional neural networks. *IEEE Geosci. Remote Sens. Lett.* **2021**, *18*, 1461–1465. [CrossRef]
59. Asse, D.; Randin, C.; Bonhomme, M.; Delestrade, A.; Chuine, I. Process-based models outcompete correlative models in projecting spring phenology of trees in a future warmer climate. *Agric. For. Meteorol.* **2020**, *285–286*, 107931. [CrossRef]
60. Alberton, B.; da Silva Torres, R.; Sanna Freire Silva, T.; Rocha, H.; SB Moura, M.; Morellato, L. Leafing patterns and drivers across seasonally dry tropical communities. *Remote Sens.* **2019**, *11*, 2267. [CrossRef]
61. Bórnez, K.; Richardson, A.; Verger, A.; Descals, A.; Peñuelas, J. Evaluation of vegetation and proba-v phenology using phenocam and eddy covariance data. *Remote Sens.* **2020**, *12*, 3077. [CrossRef]
62. Beck, P.; Atzberger, C.; Høgda, K.; Johansen, B.; Skidmore, A. Improved monitoring of vegetation dynamics at very high latitudes: A new method using MODIS NDVI. *Remote Sens. Environ.* **2006**, *100*, 321–334. [CrossRef]
63. Elmore, A.; Guinn, S.; Minsley, B.; Richardson, A. Landscape controls on the timing of spring, autumn, and growing season length in mid-Atlantic forests. *Glob. Change Biol.* **2012**, *18*, 656–674. [CrossRef]
64. Klosterman, S.; Richardson, A. Observing spring and fall phenology in a deciduous forest with aerial drone imagery. *Sensors* **2017**, *17*, 2852. [CrossRef] [PubMed]
65. Gu, L.; Post, W.; Baldocchi, D.; Black, T.; Suyker, A.; Verma, S.; Vesala, T.; Wofsy, S. Characterizing the seasonal dynamics of plant community photosynthesis across a range of vegetation types. In *Phenology of Ecosystem Processes*; Noormets, A., Ed.; Springer: New York, NY, USA, 2009; pp. 35–58.
66. Sonnentag, O.; Hufkens, K.; Teshera-Sterne, C.; Young, A.; Friedl, M.; Braswell, B.; Milliman, T.; O'Keefe, J.; Richardson, A. Digital repeat photography for phenological research in forest ecosystems. *Agric. For. Meteorol.* **2012**, *152*, 159–177. [CrossRef]
67. Roth, K.L.; Roberts, D.A.; Dennison, P.E.; Peterson, S.H.; Alonzo, M. The impact of spatial resolution on the classification of plant species and functional types within imaging spectrometer data. *Remote Sens. Environ.* **2015**, *171*, 45–57. [CrossRef]
68. Silvero, N.E.; Demattê, J.A.; Vieira, J.d.S.; Mello, F.A.d.O.; Amorim, M.T.A.; Poppiel, R.R.; Bonfatti, B.R. Soil property maps with satellite images at multiple scales and its impact on management and classification. *Geoderma* **2021**, *397*, 115089. [CrossRef]
69. Chen, X.; Ciais, P.; Maignan, F.; Zhang, Y.; Bastos, A.; Liu, L.; Zhang, H. Vapor pressure deficit and sunlight explain seasonality of leaf phenology and photosynthesis across amazonian evergreen broadleaved forest. *Glob. Biogeochem. Cycles* **2021**, *35*, e2020GB006893. [CrossRef]
70. Wu, J.; Albert, L.P.; Lopes, A.P.; Restrepo-Coupe, N.; Hayek, M.; Wiedemann, K.T.; Saleska, S.R. Leaf development and demography explain photosynthetic seasonality in Amazon evergreen forests. *Sci. (Am. Assoc. Adv. Sci.)* **2016**, *351*, 972–976. [CrossRef]

71. Fayolle, A.; Picard, N.; Doucet, J.-L.; Swaine, M.; Bayol, N.; Bénédet, F.; Gourlet-Fleury, S. A new insight in the structure, composition and functioning of central African moist forests. *For. Ecol. Manag.* **2014**, *329*, 195–205. [CrossRef]
72. Gallinat, A.S.; Ellwood, E.R.; Heberling, J.M.; Miller-Rushing, A.J.; Pearse, W.D.; Primack, R.B. Macrophenology: Insights into the broad-scale patterns, drivers, and consequences of phenology. *Am. J. Bot.* **2021**, *108*, 2112–2126. [CrossRef]
73. Pérez-Ramos, I.M.; Cambrollé, J.; Hidalgo-Galvez, M.D.; Matías, L.; Montero-Ramírez, A.; Santolaya, S.; Godoy, Ó. Phenological responses to climate change in communities of plants species with contrasting functional strategies. *Environ. Exp. Bot.* **2020**, *170*, 103852. [CrossRef]
74. Lopes, A.P.; Nelson, B.W.; Wu, J.; Graça, P.M.L.d.A.; Tavares, J.V.; Prohaska, N.; Saleska, S.R. Leaf flush drives dry season green-up of the Central Amazon. *Remote Sens. Environ.* **2016**, *182*, 90–98. [CrossRef]
75. Ide, R.; Oguma, H. Use of digital cameras for phenological observations. *Ecol. Inform.* **2010**, *5*, 339–347. [CrossRef]
76. Weil, G.; Lensky, I.; Levin, N. Using ground observations of a digital camera in the VIS-NIR range for quantifying the phenology of Mediterranean woody species. *Int. J. Appl. Earth Obs. Geoinf.* **2017**, *62*, 88–101. [CrossRef]
77. Delpierre, N.; Soudani, K.; Berveiller, D.; Dufrêne, E.; Hmimina, G.; Vincent, G. "Green pointillism": Detecting the within-population variability of budburst in temperate deciduous trees with phenological cameras. *Int. J. Biometeorol.* **2020**, *64*, 663–670. [CrossRef] [PubMed]
78. Petach, A.; Toomey, M.; Aubrecht, D.; Richardson, A. Monitoring vegetation phenology using an infrared-enabled security camera. *Agric. For. Meteorol.* **2014**, *195–196*, 143–151. [CrossRef]
79. Liang, L.; Schwartz, M.; Fei, S. Validating satellite phenology through intensive ground observation and landscape scaling in a mixed seasonal forest. *Remote Sens. Environ.* **2011**, *115*, 143–157. [CrossRef]
80. Diez, J.; Ibáñez, I.; Miller-Rushing, A.; Mazer, S.; Crimmins, T.; Crimmins, M.; Bertelsen, C.; Inouye, D. Forecasting phenology: From species variability to community patterns. *Ecol. Lett.* **2012**, *15*, 545–553. [CrossRef]
81. Ibáñez, I.; Primack, R.; Miller-Rushing, A.; Ellwood, E.; Higuchi, H.; Lee, S.; Kobori, H.; Silander, J. Forecasting phenology under global warming. *Philos. Trans. R. Soc. B Biol. Sci.* **2010**, *365*, 3247–3260. [CrossRef]
82. Gordo, O.; Sanz, J. Long-term temporal changes of plant phenology in the Western Mediterranean. *Glob. Change Biol.* **2009**, *15*, 1930–1948. [CrossRef]
83. Ke, Y.; Quackenbush, L. Review of methods for automatic individual tree-crown detection and delineation from passive remote sensing. *Int. J. Remote Sens.* **2011**, *32*, 4725–4747. [CrossRef]
84. Nagai, S.; Akitsu, T.; Saitoh, T.; Busey, R.; Fukuzawa, K.; Honda, Y.; Nasahara, K. 8 million phenological and sky images from 29 ecosystems from the Arctic to the tropics: The Phenological Eyes Network. *Ecol. Res.* **2018**, *33*, 1091–1092. [CrossRef]
85. Sethi, S.; Ewers, R.; Jones, N.; Orme, C.; Picinali, L.; Parrini, F. Robust, real-time and autonomous monitoring of ecosystems with an open, low-cost, networked device. *Methods Ecol. Evol.* **2018**, *9*, 2383–2387. [CrossRef]
86. Galán Díaz, J.; Gutiérrez-Bustillo, A.M.; Rojo, J. Influence of urbanisation on the phenology of evergreen coniferous and deciduous broadleaf trees in Madrid (Spain). *Landsc. Urban Plan.* **2023**, *235*, 104760. [CrossRef]
87. Yang, J.; Dong, J.; Liu, L.; Zhao, M.; Zhang, X.; Li, X.; Ge, Q. A robust and unified land surface phenology algorithm for diverse biomes and growth cycles in China by using harmonized landsat and sentinel-2 imagery. *ISPRS J. Photogramm. Remote Sens.* **2023**, *202*, 610–636. [CrossRef]
88. Zhang, Y.; Yin, P.; Li, X.; Niu, Q.; Wang, Y.; Cao, W.; Li, B. The divergent response of vegetation phenology to urbanization: A case study of Beijing city, China. *Sci. Total Environ.* **2022**, *803*, 150079. [CrossRef] [PubMed]
89. Bahe, M.M.; Murphy, R.L.; Russell, M.B.; Knight, J.F.; Johnson, G.R. Suitability of a single imager multispectral sensor for tree health analysis. *Urban For. Urban Green.* **2021**, *63*, 127187. [CrossRef]
90. Simović, I.; Šikoparija, B.; Panić, M.; Radulović, M.; Lugonja, P. Remote sensing of poplar phenophase and leaf miner attack in urban forests. *Remote Sens.* **2022**, *14*, 6331. [CrossRef]
91. Andreatta, D.; Bachofen, C.; Dalponte, M.; Klaus, V.H.; Buchmann, N. Extracting flowering phenology from grassland species mixtures using time-lapse cameras. *Remote Sens. Environ.* **2023**, *298*, 113835. [CrossRef]
92. Morin, X.; Roy, J.; Sonie, L.; Chuine, I. Changes in leaf phenology of three European oak species in response to climate warming. *Plant Ecol.* **2010**, *210*, 23–34.


**Disclaimer/Publisher's Note:** The statements, opinions and data contained in all publications are solely those of the individual author(s) and contributor(s) and not of MDPI and/or the editor(s). MDPI and/or the editor(s) disclaim responsibility for any injury to people or property resulting from any ideas, methods, instructions or products referred to in the content.